

# A Comparison of Proton Stopping Power Measured with Proton CT and X-Ray CT in Fresh Post-Mortem Porcine Structures

Don F. DeJongh, Ethan A. DeJongh, Victor Rykalin, Greg DeFillippo, Mark Pankuch, Andrew W. Best, George Coutrakon, Kirk L. Duffin, Nicholas T. Karonis, Caesar E. Ordoñez, Christina Sarosiek, Reinhard W. Schulte, John R. Winans, Alec M. Block, Courtney L. Hentz and James S. Welsh

**Abstract**—Currently, calculations of proton range in proton therapy patients are based on a conversion of CT Hounsfield Units of patient tissues to proton relative stopping power. Uncertainties in this conversion necessitate larger proximal and distal planned target volume margins. Proton CT can potentially reduce these uncertainties by directly measuring proton stopping power. We have used a prototype proton imaging system to acquire proton radiography and proton CT images of a sample of pork

shoulder and ribs, as well as of a pig's head. Close in time, we also acquired X-Ray CT scans, and compared proton stopping power measurements from the two modalities. We find agreement within 1% to 2% for soft tissues, and discrepancies of up to 6% for compact bone. We observe the largest discrepancies, up to 30%, for cavitated regions with mixed content of air, soft tissue, and bone, such as sinus cavities or tympanic bullae. If these results apply in general, it may be possible to substantially reduce uncertainty margins for many treatment plans, while avoiding regions with higher uncertainties. Our comparison of proton radiography data with a digitally reconstructed radiograph from the X-Ray CT demonstrates the potential of this modality for daily pre-treatment range verification.

**Index Terms**—Proton radiography, Proton computed tomography, Tomographic image reconstruction, Iterative algorithms < Tomographic image reconstruction, Performance assessment < Tomographic image reconstruction, Therapy imaging < Clinical/preclinical evaluation/application studies

Research reported in this publication was supported by the National Cancer Institute of the National Institutes of Health under award number R44CA243939.

This work has been submitted to the IEEE for possible publication. Copyright may be transferred without notice, after which this version may no longer be accessible.

Don F. DeJongh is with ProtonVDA LLC, 1700 Park St Ste 208, Naperville, IL 60563 USA (e-mail: fritz.dejongh@protonvda.com)

Ethan A. DeJongh is with ProtonVDA LLC, 1700 Park St Ste 208, Naperville, IL 60563 USA (e-mail: ethan.dejongh@protonvda.com)

Victor Rykalin is with ProtonVDA LLC, 1700 Park St Ste 208, Naperville, IL 60563 USA (e-mail: victor.rykalin@protonvda.com)

Greg DeFillippo is with Northwestern Medicine Chicago Proton Center, Warrenville, IL 60555, USA and Edward Hines Jr VA Medical Center, Radiation Oncology Service, Hines, IL 60141, USA (e-mail: greg.defillippo@nm.org)

Mark Pankuch is with Northwestern Medicine Chicago Proton Center, Warrenville, IL 60555, USA (e-mail: Mark.Pankuch@nm.org)

Andrew Best is with Department of Physics, Northern Illinois University, DeKalb, IL 60115, USA (e-mail: Z1852378@students.niu.edu)

George Coutrakon is with Department of Physics, Northern Illinois University, DeKalb, IL 60115, USA (e-mail: gcoutrakon@niu.edu)

Kirk L. Duffin is with Department of Computer Science, Northern Illinois University, DeKalb, IL 60115, USA (e-mail: kduffin@niu.edu)

Nicholas T. Karonis is with Department of Computer Science, Northern Illinois University, DeKalb, IL 60115, USA and Argonne National Laboratory, Data Science and Learning Division, Argonne, IL 60439, USA (e-mail: karonis@niu.edu)

Caesar E. Ordoñez is with Department of Computer Science, Northern Illinois University, DeKalb, IL 60115, USA (e-mail: cordonez@cs.niu.edu)

Christina Sarosiek is with Department of Physics, Northern Illinois University, DeKalb, IL 60115, USA (e-mail: csarosiek1@niu.edu)

Reinhard W. Schulte is with Loma Linda University, Loma Linda, CA 92350, USA (e-mail: rschulte@llu.edu)

John R. Winans is with Department of Computer Science, Northern Illinois University, DeKalb, IL 60115, USA (e-mail: jwinans@niu.edu)

Alec Block is with Loyola University Chicago, Loyola University Medical Center and Edward Hines Jr., VA Hospital, Stritch School of Medicine, Department of Radiation Oncology, Cardinal Bernardin Cancer Center, Maywood, IL, 60153 USA (e-mail: alblock@lumc.edu)

Courtney Hentz is with Loyola University Chicago, Loyola University Medical Center and Edward Hines Jr., VA Hospital, Stritch School of Medicine, Department of Radiation Oncology, Cardinal Bernardin Cancer Center, Maywood, IL, 60153 USA (e-mail: Courtney.Hentz@lumc.edu)

James S. Welsh is with Loyola University Chicago, Loyola University Medical Center and Edward Hines Jr., VA Hospital, Stritch School of Medicine, Department of Radiation Oncology, Cardinal Bernardin Cancer Center, Maywood, IL, 60153 USA (e-mail: James.Welsh@va.gov)

## I. INTRODUCTION

IN radiation therapy, protons provide a superior dose distribution compared to X-Rays, with a relatively low dose deposition in the entrance region (plateau), followed by a steep increase to a dose (Bragg) peak and an even steeper distal dose fall-off. Treatment planning for proton therapy starts with an X-Ray CT image with voxel values measured in Hounsfield units (HU), converted to proton relative stopping power (RSP), relative to water, using scanner-specific calibrations. There is no consistent one-to-one relationship between HU and RSP for different tissues and materials, leading to significant range uncertainties [1], typically quantified as  $3.5\% \pm 1$  mm for treatment planning purposes at the Northwestern Medicine Chicago Proton Center (NMCPC).

Treatment planning procedures take these uncertainties into account with measures including adding uncertainty margins, selection of beam angles tangential to organs at risk, and robust optimization. Using dose delivery technology such as Pencil Beam Scanning (PBS) and intensity modulation, the resulting plans are robust to the uncertainties and provide major benefits to a significant fraction of patients [2]. However, they increase the high-dose treatment volume and can preclude use of the most advantageous beam angles. In the quest to further optimize proton therapy while also reducing costs, proton beam-based image guidance is often considered to be a prerequisite to achieve the full potential of proton therapy [3]. This is particularly the case for hypo-fractionated treatments,

which can benefit from more conformal dose distributions and a higher standard of safety given the high dose delivery for each treatment.

Proton CT (pCT) will substantially reduce the uncertainties of treatment planning by directly measuring RSP, and provides further benefits including lack of artifacts from metallic implants, and much lower dose to the patient than comparable x-ray images [4]. Proton radiography (pRad) has the potential to provide a fast and efficient check of patient set up and integrated range along a beam's eye view just before treatment [5], [6]. A comparison of a pRad with a digitally-reconstructed radiograph (DRR) based on projections through the 3D RSP map used for treatment planning can reveal discrepancies from range uncertainties as well as other sources such as anatomical changes.

In a recent publication, Deffet *et al.* have assessed the accuracy of HU to RSP conversion with a pRad of a pig's head [7]. Using a detector that integrates the contribution of every proton during the irradiation of a pencil beam shot, they applied a deconvolution algorithm to improve the spatial resolution to better than the pencil beam size, and registered the resulting pRad with an X-Ray CT. Comparing the pRad to the expectation from the CT, they find range uncertainties generally well below the usual safety margins by about a factor of five, with the exception of regions including sinus cavities, where the range discrepancies are large.

Meijers *et al.* have studied range uncertainties in porcine samples of head, thorax, and femur using a range probing technique [8]. They find a maximum discrepancy of 0.75 relative to their uncertainty margin prescription. A study of 2025 proton spots acquired during different breathing phases with a set of inflatable porcine lungs [9] finds a mean relative range error of 1.2% with a spread of 2.3% (1.5 standard deviations).

Bär *et al.* experimentally compared dual-energy CT (DECT) performance against conventional single-energy CT (SECT) for proton treatment planning by comparing 12 tissue-equivalent plastic materials and 12 fresh heterogeneous animal tissue samples in terms of water equivalent range predictions of 195 MeV protons [10]. While they found that SECT performs very well in soft tissues with somewhat larger deviations in bone, their results showed better performance of DECT compared to SECT in all materials.

We present herein measurements of RSP in a fresh post-mortem pig's head as well as a sample of pork shoulder and ribs, comparing the RSP determination from proton images and X-Ray CT images taken close in time. In contrast to [7] we obtain proton images with a list-mode proton imaging system, which measures trajectories and residual ranges of individual protons. Tracking detectors measure the transverse positions of individual protons before and after the patient, and a residual range detector determines the proton energy absorbed within the object. Proton trajectories deviate from straight lines due to multiple Coulomb scattering, and the list-mode approach helps reduce resulting blurring. In addition, we obtain pCT images as well as pRad images. The pCT image reconstruction enables us to define 3D regions of interest (ROI) and directly assess the RSP of different tissues in the porcine structures. In addition



Fig. 1. The ProtonVDA system [11], positioned in the horizontal beam treatment room at the NMCPC. The rotating platform between the tracking planes enabled imaging with a full set of angles relative to the PBS system, and was used with a pig's head (as shown) as well as with the pork shoulder and ribs shown on the right.

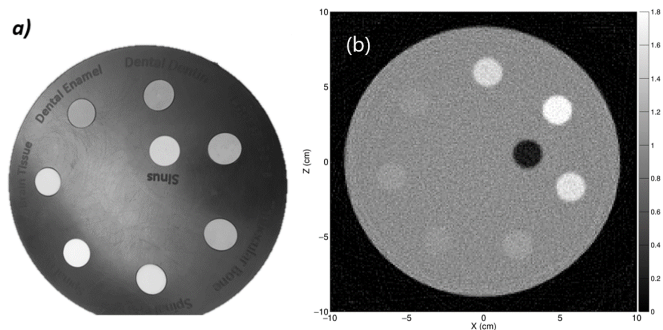


Fig. 2. (a) Custom phantom with eight 4 cm thick, 1.8 cm diameter inserts of various tissue-equivalent materials with known RSP. (b) One slice of the reconstructed pCT image.

to reporting the average RSP of the voxels in each ROI, we report the standard deviation (SD) of the RSP distribution for the voxels in each ROI.

## II. MATERIALS AND METHODS

We obtained proton images with the prototype ProtonVDA proton imaging system [11], shown in Fig. 1 positioned in a horizontal beam line equipped with PBS at the NMCPC. This system is capable of automatically acquiring data from a low-intensity proton beam delivered by the PBS system and reconstructing pRad images [12] with the pRad algorithm described in [13]. While we are in the process of extending this automatic capability to pCT, for the current work we used the rotational platform shown in Fig. 1, and acquired data in 90 separate segments with a  $4^\circ$  rotation between segments to provide the full set of angles required for pCT. As described in [11], our pRad system uses multiple incoming proton energies for a single image, and we acquired data with multiple energies at each angle. For each proton, we calculate a Water-Equivalent Path Length (WEPL) and Most Likely Path (MLP). We reconstructed the pCT images using the least-squares iterative algorithm described in [14], which provides assurance that the iterative solution has converged with a fit

TABLE I  
COMPARISON OF THE RSP MEASURED USING pCT TO THE KNOWN RSP,  
FOR THE TISSUE-EQUIVALENT INSERTS IN THE PHANTOM IN FIG. 2.

Insert	pCT RSP (SD)	Known RSP	Diff. %
Sinus	0.192 (0.094)	0.200	-4.0
Enamel	1.768 (0.086)	1.755	0.7
Dentin	1.504 (0.083)	1.495	0.6
Brain	1.043 (0.078)	1.040	0.3
Spinal Cord	1.046 (0.071)	1.040	0.6
Spinal Disk	1.079 (0.075)	1.070	0.8
Trabecular Bone	1.106 (0.079)	1.100	0.5
Cortical Bone	1.570 (0.084)	1.555	1.0

to the data that is close to optimal within the statistical power of the data. In order to analyze the images with the statistical noise inherent in our data, we have not applied any smoothing. While smoothing can make the images look less noisy and can be beneficial for clinical visualization, it can result in unknown systematic effects in the presence of rapid RSP variations.

We tested the accuracy of our pCT images with the custom cylindrical phantom shown in Fig. 2, which incorporates a set of tissue-equivalent inserts with known RSP, as measured with a multi-layer ionization chamber used for range calibrations at NMCPC by observing the pull-back of a 150 MeV beam with and without the material. The pCT image of the phantom used approximately 20 million protons taken at incoming energies of 118, 160, and 187 MeV to reconstruct a volume of  $200 \times 60 \times 200$  1 mm<sup>3</sup> voxels. The results in Table I demonstrate an RSP accuracy better than 1% with the exception of a 4% discrepancy for the sinus insert. However, this insert has very low density, and the discrepancy in terms of RSP is only 0.008. The SD values show that our RSP measurements per voxel have a statistical noise of typically 7%. Future measurements with the automated system will enable convenient acquisition of larger data sets with reduced noise.

We assembled two fresh post-mortem porcine structures for proton imaging, both shown in Fig. 1, from samples available and packaged at a butcher's shop. The first is a sample of pork shoulder and pork ribs, with the ribs partially surrounding the shoulder, and the combination inserted into a blue wax cylinder with an inner radius of 20 cm. The pCT images used an approximate total of 180 million protons at energies of 120, 160, 185, and 203 MeV to reconstruct a volume of  $250 \times 250 \times 250$  1 mm<sup>3</sup> voxels.

A pig's head provided a more complex structure, which we immobilized on the platform with plastic foam and tape, with four 4 mm CT markers mounted on the packaging. This pCT reconstruction used approximately 150 million protons at energies of 120, 160, 200, and 220 MeV for a volume of  $300 \times 250 \times 300$  1 mm<sup>3</sup> voxels.

We obtained X-Ray CT images of the porcine structures close in time to the pCT images. To keep the anatomy consistent, we acquired the X-Ray CT scans in the same orientation using a clinical vertical (horizontal-plane) CT scanner.

Both pCT images used an estimated dose of 1-2 mGy, compared to an estimated 20-30 mGy for the X-Ray CT scans. This shows that pCT images could be made with much lower

noise than the ones presented in this study while still using a lower dose than an X-Ray CT. Lower noise may not be necessary, however, since the errors from individual voxels are averaged out when calculating range to a target.

We used the Velocity [15] clinical image staging program to perform a rigid registration of corresponding X-Ray CT and pCT scans, resample them into the same voxel space, and define identical ROIs for each by drawing contours slice-by-slice in several segments of tissue. For the X-Ray CT scan, we used the RayStation treatment planning program [16] with the scanner-specific calibration to convert the HU values into RSP. For each ROI, we calculated the mean and SD of the RSPs of the voxels within the contours.

### III. COMPARISON OF PRAD WITH X-RAY CT FOR THE PIG'S HEAD

In the case of the pig's head, we obtained a pRad image using our automated system in addition to the pCT data. The pRad used approximately 20 million protons of the same four energies as the pCT. We produced a DRR to compare with the pRad, starting with the X-Ray CT scan registered to the pCT. Using the TOPAS simulation software [17][18], we read in the X-Ray CT data, applied the Hounsfield-to-RSP conversion for the NMCPC CT scanner, and generated protons to simulate our pRad. The simulation defined the isocentric reference frame and proton directions in that frame to match the beam line at NMCPC, and positioned the simulated pig's head to match the position we used for the pRad data acquisition. This positioning required some fine-tuning to optimize the difference image between the pRad and the DRR. Similarly as in [6], we find that rotations of 0.5° or translations of 0.5 mm produce noticeable discrepancies.

The resulting DRR is shown in Fig. 3(b), which we then compared to the real pRad in Fig. 3(a) to produce the difference image shown in Fig. 3(c). The difference map subtracts the water equivalent thickness (WET) predicted by the virtual DRR from the WET measured by pRad, with red showing a higher measured WET and blue showing a lower measured WET. Large differences are observed around the edges of the head and other areas of rapid variation which are most sensitive to a precise alignment of the two images. The four CT markers are visible in the difference map at coordinates near (-9,1), (3,0), (3,9), and (11,10) cm. These markers are designed to show up brightly in X-Rays, but don't have a correspondingly high RSP. They are well-aligned in the difference image and appear with net negative WET values. The slight difference of about 1 mm observed in the air around the pig's head is likely due to a calibration issue for the 120 MeV protons that travelled deep inside the scintillator. There is also a grid structure visible in the background; this is an artifact due to non-uniformities in the construction of the tracking plane. We are currently upgrading the system, and expect to correct these issues in the next version.

Most regions of the head, including the brain and neck muscle, show agreement within 1-2 mm of WET between the DRR and pRad, in comparison to a total WET of up to 200 mm, confirming previous observations that the standard

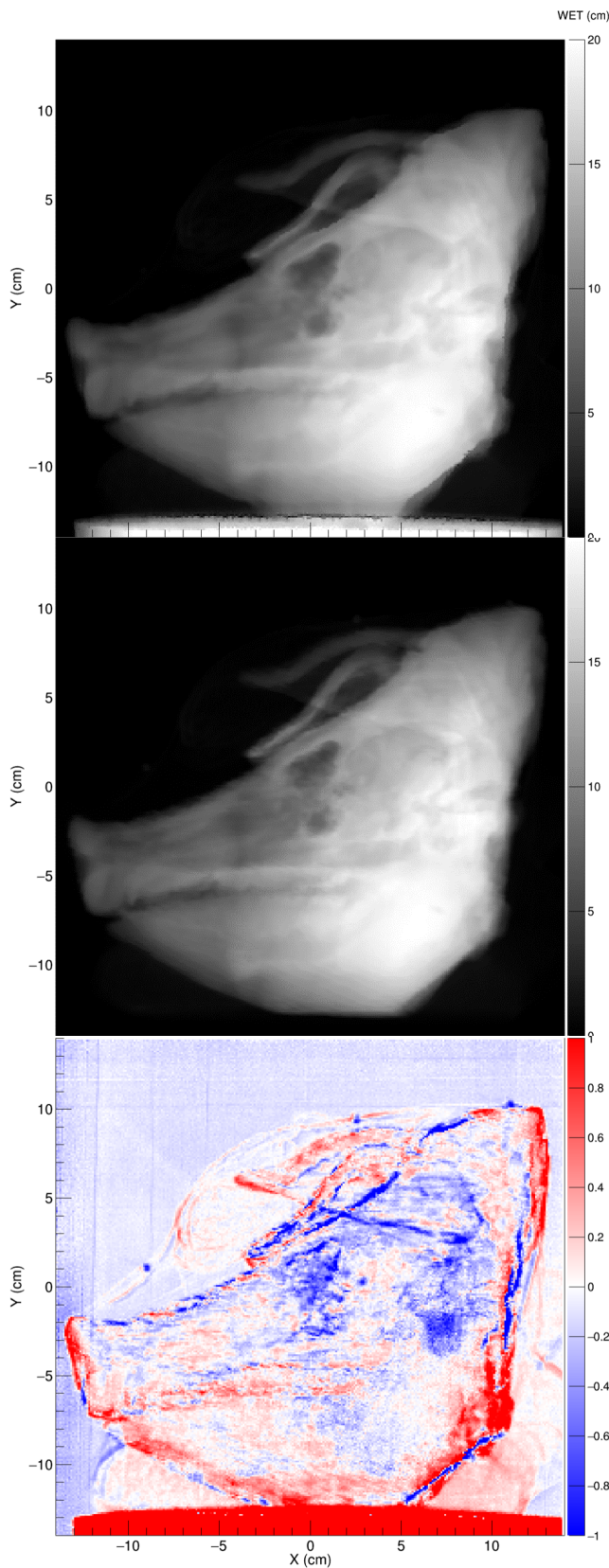


Fig. 3. (a) Proton radiograph of the pig's head. (b) DRR of the pig's head based on an X-Ray CT scan. (c) Difference between the proton radiograph and DRR. Notable differences are visible in the sinus region near coordinates (0,0) and the tympanic bullae near coordinates (8,-2).

TABLE II  
COMPARISON RESULTS FOR A SAMPLE OF PORK SHOULDER AND RIBS.

Region	Volume cm <sup>3</sup>	pCT		X-Ray CT		Diff. %
		RSP	(SD)	RSP	(SD)	
Air	3.7	0.070	(0.070)	0.006	(0.003)	
Adipose Shoulder	6.6	0.983	(0.086)	0.977	(0.005)	0.6
Adipose Rib	1.2	0.965	(0.054)	0.967	(0.007)	-0.2
Muscle Shoulder-Med	17.5	1.044	(0.112)	1.046	(0.005)	-0.2
Muscle Shoulder-Lat	25.6	1.043	(0.114)	1.043	(0.005)	0.0
Muscle Rib	5.8	1.051	(0.091)	1.046	(0.005)	0.5
Trabecular Bone Rib	1.1	1.120	(0.062)	1.141	(0.013)	-1.9
Trabecular Shoulder	1.1	1.116	(0.082)	1.114	(0.021)	0.2
Compact Bone	0.4	1.467	(0.127)	1.568	(0.035)	-6.9
Blue Wax	6.2	0.972	(0.114)	0.932	(0.008)	4.1

HU to RSP conversions work very well. The most notable anatomical WET differences are in the sinus region and the tympanic bullae, where the measured WET from pRad is 4 to 8 mm lower than the expected WET from the X-Ray CT. The sinus result is similar to that reported for a pig's head in [7], while their image does not contain the tympanic bullae. The sinus and tympanic bullae are similar in that they are both heterogeneous regions with large variations in density and composition, suggesting that conversions from X-Ray Hounsfield units to RSP may be less accurate in such structures than in more uniform ones. There are also hints of discrepancies in bony regions include the skull and mandible.

#### IV. RESULTS FOR PORK SHOULDER AND RIBS

We analyzed RSP differences between pCT and X-Ray CT for 10 different regions in the pork ribs/shoulder structure, with examples of regions for one slice indicated in Fig. 4. We found differences of 0.6% or less for all soft tissues, both muscle and adipose, as shown in Table II. We see a slightly more significant difference of 1.9% in the rib trabecular bone, and a much larger difference of 6.9% in the compact bone. The 4.1% difference in the blue wax surrounding the sample is not surprising, as the Hounsfield-to-RSP conversion was not calibrated for that type of material.

Due to multiple Coulomb scattering of the imaging protons, the X-Ray image appears much sharper, as shown in the single slice comparison in Fig. 4, but the pCT image is still sharp enough to distinguish compact bone from soft bone and provides enough contrast to distinguish between muscle tissue and fatty tissue. The pCT image is much noisier, but this can be mitigated by using more protons.

#### V. RESULTS FOR PIG'S HEAD

Examples of regions for one slice each in two views of the pig's head are indicated in Fig. 5. Following a similar pattern to the results from the pork shoulder and ribs, our analysis of RSP from pCT and X-Ray CT for the pig's head shows larger differences between pCT and X-Ray CT for bone structures than for soft structures, with differences even higher in dense bone than in soft bone, as shown in Table III. In the case of the sinus, our ROI encompasses a small volume of air. In the case of the tympanic bullae, shown in Fig 6, the ROI encompasses a larger volume containing a heterogeneous mixture, and we

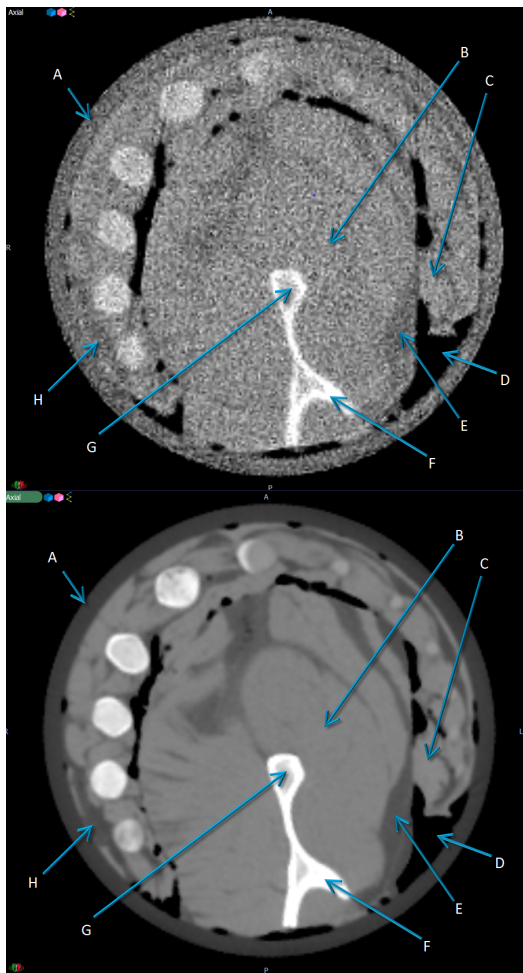


Fig. 4. Examples of 1 mm thick CT slices for the pork shoulder and ribs, showing regions of interest. Top: pCT. Bottom: X-Ray CT. Labels are: A: Blue Wax. B: Muscle (Shoulder). C: Muscle (Ribs). D: Air. E: Adipose Shoulder. F: Compact Bone. G: Trabecular Bone Shoulder. H: Adipose Ribs.

find overall a much larger discrepancy - 30% - than for any other structure we examined.

Fig. 7 shows a comparison of averages of ten 1 mm slices from the side of the pig's head for pCT and X-Ray CT, in order to reduce noise and allow us to see systematic differences in RSP more clearly. Features are slightly blurred due to their change in shape with depth. Also, the grey scale is calibrated in terms of RSP, whereas in Fig. 5 and 6 it was adjusted visually to optimize contouring. These particular slices highlight the tympanic bullae, which are very distinct in the different image Fig. 7(c), as they are for the pRad in Fig 3. While Fig. 3(c) shows a similar difference in WET in the sinus region, Fig. 7(c) shows less of a difference in RSP in this particular slice of the sinus.

The difference map also clearly shows the systematic discrepancy in the skull bone and the mandible, while the brain and muscle regions show good agreement. The difference in the tip of the snout is caused by an incomplete set of data through that area. The pencil beam scans used for the pCT data only covered a  $25 \times 25 \text{ cm}^2$  area, so the tip of the snout was not quite covered at lateral angles.

TABLE III  
COMPARISON RESULTS FOR THE PIG'S HEAD.

Region	Volume cm <sup>3</sup>	pCT		X-Ray CT		Diff. %
		RSP	(SD)	RSP	(SD)	
Sinus Air	0.1	0.089	(0.093)	0.038	(0.009)	
Tympanic Bullae	5.2	0.56	(0.28)	0.73	(0.57)	-30
Adipose	5.4	0.936	(0.180)	0.951	(0.003)	-1.6
Eye Right	0.9	1.009	(0.148)	1.014	(0.005)	-0.5
Eye Left	0.7	1.022	(0.124)	1.015	(0.005)	0.7
Brain Stem	1.5	1.010	(0.188)	1.017	(0.008)	-0.7
Brain	8.7	1.027	(0.178)	1.031	(0.008)	-0.4
Tongue	9.4	1.048	(0.238)	1.031	(0.014)	1.6
Muscle	7.5	1.046	(0.209)	1.052	(0.012)	-0.6
Lens	0.1	1.093	(0.124)	1.075	(0.005)	1.6
Bone Skull	3.6	1.263	(0.159)	1.308	(0.033)	-3.6
Mandible	0.4	1.488	(0.192)	1.582	(0.027)	-6.3

## VI. DISCUSSION

Our results confirm several recent reports [7][8][9][10] indicating that it may be possible to reduce the standard uncertainty margins used in proton therapy. For example, our pRad and pCT images of the pig's head show that the RSP map derived from the X-Ray CT is generally accurate, although with discrepancies in some regions such as the sinus and tympanic bullae. Proton beam therapy can be useful for radiotherapeutic management of many head and neck and intracranial malignancies. Surgical resection is considered the standard of care for most sinonasal cancers, however, it is rarely used as the only treatment modality. Clinical data leads us to believe that there is room for improvement with proton beam therapy and reduced margins, with the possibility of safely escalating dose to improve local control while maintaining the lower rates of toxicity imparted by proton beam therapy.

Among the classic head and neck examples for which proton beam radiation therapy appears especially useful are esthesioneuroblastoma (olfactory neuroblastoma), sinonasal undifferentiated carcinoma (SNUC) and some challenging nasopharyngeal carcinoma cases. In such cases, proton beam therapy can offer additional sparing of critical adjacent sensitive structures, such as the globe, optic nerves, optic chiasm and brain compared to conventional photon-based external beam radiation therapy [19]. This is needed since, for instance, the conventional radiation therapy literature on esthesioneuroblastoma reports severe ocular radiation injury leading to a poor or nonfunctioning eye at rates ranging from 8% to 24% [20][21][22].

In a series of nine patients with esthesioneuroblastomas and neuroendocrine tumors treated with induction chemotherapy followed by proton beam therapy and a median follow up of 20.5 months, Bhattacharyya *et al.* noted only a single and transient ocular complication [23]. With a more prolonged follow-up of 40 months, Nishimura *et al.* reported no toxicities greater than grade 2 in their series of esthesioneuroblastomas treated with proton therapy in Chiba, Japan [24]. In their experience with neuroendocrine tumors of the sinonasal tract and esthesioneuroblastomas, Fitzek *et al.* reported no significant ocular complications, although four patients developed grade 2 or 3 radiation injury to the frontal lobes [25]. The Massachusetts

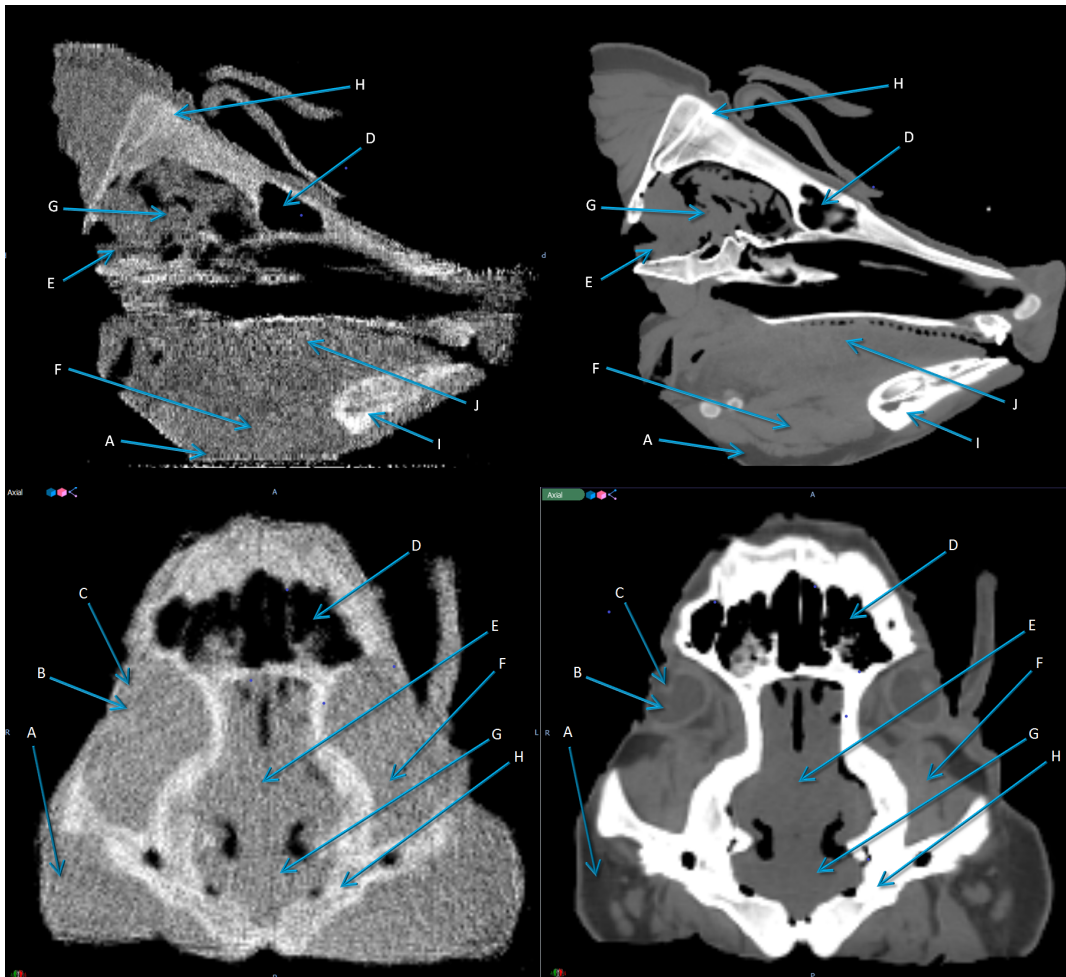


Fig. 5. Examples of 1 mm thick CT slices for the Pig's head, showing regions of interest. Top row: sagittal view. Bottom row: coronal view. Images on the left are for pCT, those on the right are for X-Ray CT. Labels are: A: Adipose. B: Eye. C: Lens. D: Sinus. E: Brain Stem. F: Muscle. G: Brain. H: Bone Skull. I: Mandible. J: Tongue.

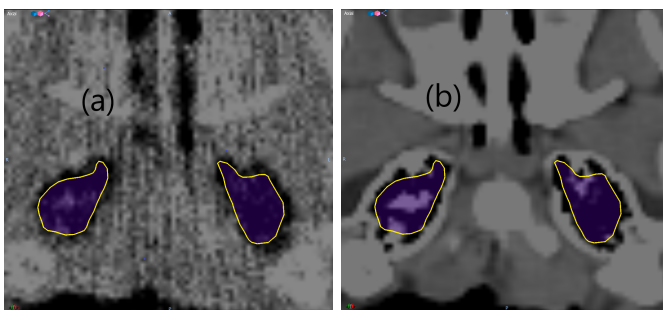


Fig. 6. Tympanic bullae contours in one CT slice. (a) pCT. (b) X-Ray CT.

General Hospital and Massachusetts Eye and Ear Infirmary team initially reported on 10 patients with esthesioneuroblastoma who underwent craniofacial resection and adjuvant proton beam radiation (with or without chemotherapy) [26]. Based on their encouraging results, the team later reported the updated results with an additional five years of experience and a doubling of the cohort [27]. Twenty-two patients (10 with Kadish stage B disease and 12 with Kadish stage C

disease) and an average follow-up of 73 months were treated with craniofacial resection followed by proton beam therapy with or without chemotherapy. The 5-year disease-free and overall survival rates were 86.4% and 95.2%, respectively. Only one patient experienced severe late-radiation toxicity. In a series of sixty-nine patients with various sinonasal tumors (including squamous cell carcinoma, adenoid cystic carcinoma, esthesioneuroblastoma, adenocarcinoma, small cell neuroendocrine carcinoma, sinonasal undifferentiated carcinoma) who underwent definitive proton beam therapy on the Proton Collaborative Group registry study between 2010 and 2016, late toxicities occurred in 15% of patients but there were no grade toxicities greater than grade 2. No patients developed vision loss or symptomatic brain necrosis [28].

Despite the relative safety of proton therapy, the predominant pattern of failure remains local recurrence. For instance, the University of Florida group reported that local recurrence accounted for 60.7% of the failures [29]. Russo et al similarly reported a predominantly pattern of failure in their sinonasal squamous cell carcinoma patients [30]. However, squamous cell carcinoma is sometimes considered a higher risk histology in sinonasal tumors. Although it did not reach statistical

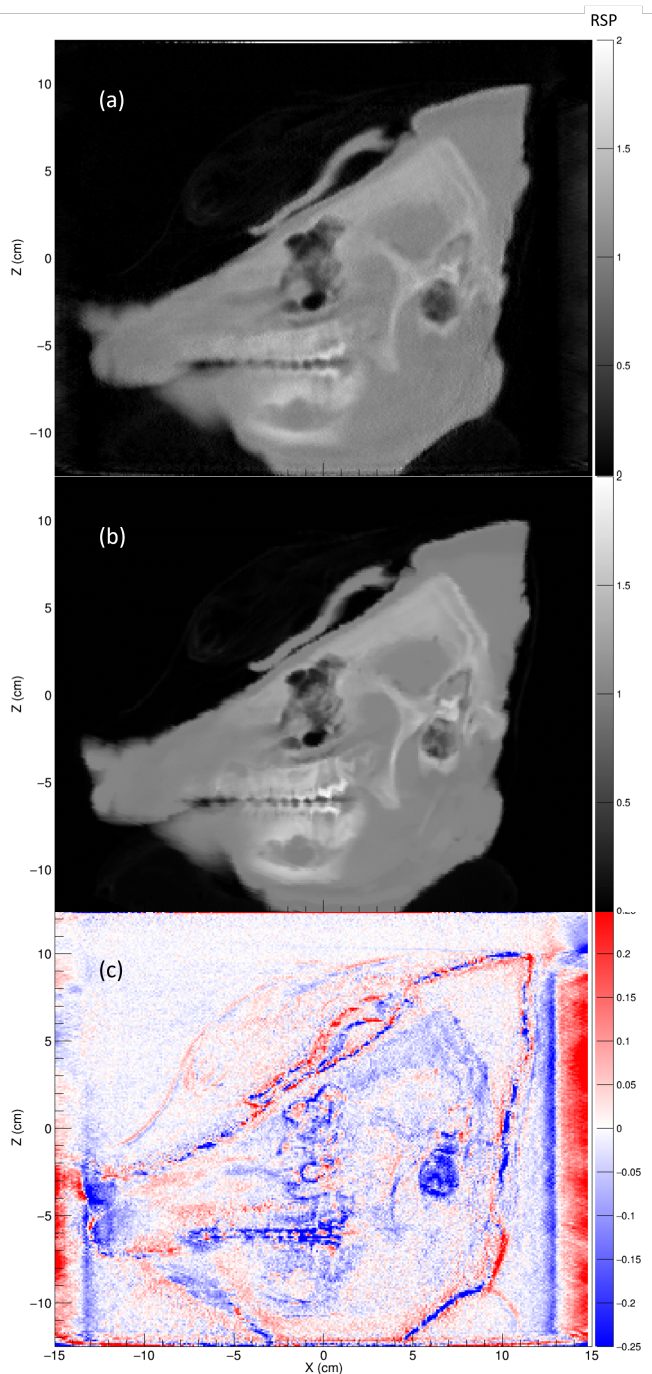


Fig. 7. Ten-slice averages (a) From pig's head pCT. (b) From pig's head X-Ray CT. (c) Proton - X-Ray difference.

significance, the University of Florida team also reported worse 3-year overall survival rates for their squamous cell carcinoma patients compared to other histologies [29].

A retrospective analysis of SNUC patients was done by a team in Japan at the Hyogo Ion Beam Center to evaluate the efficacy and safety of proton therapy. Among their 9 patients, the 2-year overall survival, progression-free survival, and local control rates were 78%, 33%, and 71%, respectively. No patients experienced any severe late toxicity. However, 7 patients (78%) developed recurrence by the time of the publi-

cation. The authors felt that although proton beam therapy was effective and safe, the local recurrence rates were unsatisfactory and adjuvant therapy with chemotherapy/immunotherapy should be considered [26]. These are examples where safely escalating dose, while decreasing margins, could improve local control while diminishing side-effects.

As an example of a specific successful case, Thekkedath *et al.* reported the case of a 31-year-old Bosnian male who presented with headaches, facial pain, and epistaxis who was found to have a very large SNUC. The patient experienced near complete resolution of his stage IVB (T4b N0 M0) SNUC after treatment with combination chemotherapy (cisplatin and gemcitabine followed by weekly cisplatin) in combination with proton therapy [31]. This illustrates the potential of proton beam therapy, however SNUC is a difficult cancer to conquer and refinements in dose delivery will help ensure similar outcomes in a larger fraction of cases.

Comparisons between pRad images, which could potentially be done with an efficient workflow on a daily basis before each treatment, and DRRs from the planning CT, as for the example in Fig. 3, could help provide assurance that treatment plans using reduced margins are safe. Furthermore, it may be possible to use one or more pRad images to improve the planning CT, and several recent studies have explored methods to use pRad images to produce patient-specific CT calibrations [32][33][34][35] and more accurate RSP maps. In this scenario, proton imaging might be used for pRad much more than for pCT. However, we note that the capabilities of a pCT system will still be needed in order to relate data from one or more pRad images to the planning CT. Furthermore, there will remain cases where a full pCT image will be useful, such as with patients with metallic implants.

## VII. CONCLUSION

In a comparison of proton stopping power as measured directly with proton imaging to values obtained from X-Ray CT scans, we find agreement within 1% to 2% for soft tissues, and discrepancies of up to 6% for compact bone. We observe the largest discrepancies, up to 30%, for cavitated regions with mixed content of air, soft tissue, and bone, such as sinus cavities or tympanic bullae. If these results apply in general, it may be possible to substantially reduce uncertainty margins for many treatment plans, while avoiding regions with higher uncertainties. Our comparison of proton radiography data with a digitally reconstructed radiograph from the X-Ray CT demonstrates the potential of this modality for daily pre-treatment range verification.

## ACKNOWLEDGMENT

The authors thank Aditya Panchal of Amita Health for assistance with saving pCT images into DICOM format. We thank the staff of NMCPC for assistance with and use of the treatment room and X-Ray CT scanner. We thank the staff of Ion Beam Applications for assistance with proton beam operations, including the work of Nick Detrich to produce custom pencil beam scanning patterns. We thank Igor Polnyi of ProtonVDA for his help assembling the detector and operations during data collection.

## REFERENCES

- [1] H. Paganetti, "Range uncertainties in proton therapy and the role of monte carlo simulations," *Physics in Medicine and Biology*, vol. 57, no. 11, pp. R99–R117, may 2012. [Online]. Available: <https://doi.org/10.1088/0031-9155/57/11/R99>
- [2] A. J. Lomax, "Myths and realities of range uncertainty," *The British Journal of Radiology*, vol. 93, no. 1107, p. 20190582, 2020, pMID: 31778317. [Online]. Available: <https://doi.org/10.1259/bjr.20190582>
- [3] A. N. Schreuder and J. Shamblin, "Proton therapy delivery: what is needed in the next ten years?" *The British Journal of Radiology*, vol. 93, no. 1107, p. 20190359, 2020, pMID: 31692372. [Online]. Available: <https://doi.org/10.1259/bjr.20190359>
- [4] R. W. Schulte, V. Bashkurov, M. C. Loss Klock, T. Li, A. J. Wroe, I. Evseev, D. C. Williams, and T. Satogata, "Density resolution of proton computed tomography," *Medical Physics*, vol. 32, no. 4, pp. 1035–1046, 2005. [Online]. Available: <https://aapm.onlinelibrary.wiley.com/doi/abs/10.1118/1.1884906>
- [5] C. Miller, B. Altoos, E. DeJongh, M. Pankuch, D. DeJongh, V. Rykalin, C. Ordoñez, N. Karonis, J. Winans, G. Coutrakon, and J. Welsh, "Reconstructed and real proton radiographs for image-guidance in proton beam therapy," *Journal of Radiation Oncology*, vol. 8, pp. 97–101, 03 2019.
- [6] M. Pankuch, E. DeJongh, F. DeJongh, and et al., "A method to evaluate the clinical utility of proton radiography for geometric patient alignment," in *Proceedings of the 57th Annual Meeting of the Particle Therapy Cooperative Group (PTCOG)*, May 2018, available: <http://theijpt.org/doi/pdf/10.14338/2331-5180-5-2-000>.
- [7] S. Deffet, M. Cohilis, K. Souris, K. Salvo, T. Depuydt, E. Sterpin, and B. Macq, "openpr - a computational tool for ct conversion assessment with proton radiography," *Medical Physics*, vol. n/a, no. n/a, 2020. [Online]. Available: <https://aapm.onlinelibrary.wiley.com/doi/abs/10.1002/mp.14571>
- [8] A. Meijers, J. Free, D. Wagenaar, S. Deffet, A. C. Knopf, J. A. Langendijk, and S. Both, "Validation of the proton range accuracy and optimization of CT calibration curves utilizing range probing," *Physics in Medicine & Biology*, vol. 65, no. 3, p. 03NT02, feb 2020. [Online]. Available: <https://doi.org/10.1088/1361-6560/ab66e1>
- [9] A. Meijers, O. C. Seller, J. Free, D. Bondesson, C. S. Oria, M. Rabe, K. Parodi, G. Landry, J. A. Langendijk, S. Both, C. Kurz, and A. Knopf, "Assessment of range uncertainty in lung-like tissue using a porcine lung phantom and proton radiography," *Physics in Medicine & Biology*, vol. 65, no. 15, p. 155014, jul 2020. [Online]. Available: <https://doi.org/10.1088/1361-6560/ab91db>
- [10] E. Bär, A. Lalonde, R. Zhang, K.-W. Jee, K. Yang, G. Sharp, B. Liu, G. Royle, H. Bouchard, and H.-M. Lu, "Experimental validation of two dual-energy ct methods for proton therapy using heterogeneous tissue samples," *Medical Physics*, vol. 45, no. 1, pp. 48–59, 2018. [Online]. Available: <https://aapm.onlinelibrary.wiley.com/doi/abs/10.1002/mp.12666>
- [11] E. A. DeJongh, D. F. DeJongh, I. Polnyi, V. Rykalin, C. Sarosiek, G. Coutrakon, K. L. Duffin, N. T. Karonis, C. E. Ordoñez, M. Pankuch, J. S. Welsh, and J. R. Winans, "Technical note: A prototype clinical proton radiography system," 2020, arXiv:2009.04652 [physics.med-ph].
- [12] C. Sarosiek, E. A. DeJongh, G. Coutrakon, D. F. DeJongh, K. L. Duffin, N. T. Karonis, C. E. Ordoñez, M. Pankuch, V. Rykalin, J. S. Welsh, and J. R. Winans, "A prototype proton radiography system for clinical use," 2020, arXiv:2009.04657 [physics.med-ph].
- [13] C. Ordoñez, N. Karonis, K. Duffin, J. Winans, E. DeJongh, D. DeJongh, G. Coutrakon, N. Myers, M. Pankuch, and J. Welsh, "Fast in situ image reconstruction for proton radiography," *Journal of Radiation Oncology*, 05 2019.
- [14] D. F. DeJongh and E. A. DeJongh, "An iterative least squares method for proton ct image reconstruction," 2020.
- [15] *Velocity AI. (3.1.0)*, Velocity Medical Solutions.
- [16] *RayStation 9A - Clinical. (9.0.0.113)*, RaySearch Laboratories.
- [17] J. Perl, J. Shin, J. Schumann, B. Faddegon, and H. Paganetti, "TOPAS: An innovative proton Monte Carlo platform for research and clinical applications," *Medical Physics*, vol. 39, p. 6818, 2012.
- [18] B. Faddegon, J. Ramos-Mendez, J. Schuemann, A. McNamara, J. Shin, J. Perl, and P. H., "The TOPAS Tool for Particle Simulation, a Monte Carlo Simulation Tool for Physics, Biology and Clinical Research," *Physica Medica*, 2020.
- [19] A. Nichols, A. Chan, W. Jr, F. Barker, D. Deschler, and D. Lin, "Esthesioneuroblastoma: The massachusetts eye and ear infirmary and massachusetts general hospital experience with craniofacial resection, proton beam radiation, and chemotherapy," *Skull base : official journal of North American Skull Base Society ... [et al.]*, vol. 18, pp. 327–37, 10 2008.
- [20] J. Simon, W. Zhen, T. McCulloch, H. Hoffman, A. Paulino, N. Mayr, and J. Buatti, "Esthesioneuroblastoma: The university of iowa experience 1978-1998," *The Laryngoscope*, vol. 111, pp. 488 – 493, 03 2001.
- [21] P. Dulguerov and T. Calcaterra, "Esthesioneuroblastoma: The ucla experience 1970-1990," *The Laryngoscope*, vol. 102, pp. 843–9, 09 1992.
- [22] S.-K. Hwang, S.-H. Paek, D. Kim, Y.-K. Jeon, J. Chi, and H.-W. Jung, "Olfactory neuroblastomas: Survival rate and prognostic factor," *Journal of neuro-oncology*, vol. 59, pp. 217–26, 10 2002.
- [23] N. Bhattacharyya, A. Thornton, M. Joseph, M. Goodman, and P. Amrein, "Successful treatment of esthesioneuroblastoma and neuroendocrine carcinoma with combined chemotherapy and proton radiation: Results in 9 cases," *Archives of otolaryngology-head and neck surgery*, vol. 123, pp. 34–40, 02 1997.
- [24] H. Nishimura, T. Oginio, M. Kawashima, K. Nihei, S. Arahira, M. Onozawa, S. Katsuta, and T. Nishio, "Proton-beam therapy for olfactory neuroblastoma," *International journal of radiation oncology, biology, physics*, vol. 68, pp. 758–62, 07 2007.
- [25] M. Fitzek, A. Thornton, M. Varvares, M. Ancukiewicz, J. McIntyre, J. Adams, S. Rosenthal, M. Joseph, and P. Amrein, "Neuroendocrine tumors of the sinonasal tract. results of a prospective study incorporating chemotherapy, surgery, and combined proton-photon radiotherapy," *Cancer*, vol. 94, pp. 2623–34, 06 2002.
- [26] K. Morimoto, M. Murakami, D. Miyawaki, Y. Niwa, Y. Demizu, and Y. Hishikawa, "Sp408  $\hat{\text{a}}$ € proton therapy against sinonasal undifferentiated carcinoma," *Otolaryngology-head and Neck Surgery - OTOLARYNGOL HEAD NECK SURG*, vol. 141, 09 2009.
- [27] M. Herr, R. Sethi, J. Meier, K. Chambers, A. Remensneider, A. Chan, W. Curry, F. Barker, D. Deschler, and D. Lin, "Esthesioneuroblastoma: An update on the massachusetts eye and ear infirmary and massachusetts general hospital experience with craniofacial resection, proton beam radiation, and chemotherapy," *Journal of Neurological Surgery Part B: Skull Base*, vol. 75, pp. 058–064, 02 2013.
- [28] N. Yu, M. Gamez, W. Hartsell, H. Tsai, G. Laramore, G. Larson, C. Simone, C. Rossi, S. Katz, M. Buras, M. Golafshar, C. Vargas, and S. Patel, "A multi-institutional experience of proton beam therapy for sinonasal tumors," *Advances in Radiation Oncology*, vol. 4, 07 2019.
- [29] R. Dagan, C. Bryant, z. Li, D. Yeung, J. Justice, P. Dzieglewski, J. Werning, R. Fernandes, P. Pircousis, D. Lanza, C. Morris, and W. Mendenhall, "Outcomes of sinonasal cancer treated with proton therapy," *International Journal of Radiation Oncology\*Biolog\*Physics*, vol. 95, 02 2016.
- [30] A. Russo, J. Adams, E. Weyman, P. Busse, S. Goldberg, M. Varvares, D. Deschler, D. Lin, T. Delaney, and A. Chan, "Long-term outcomes after proton beam therapy for sinonasal squamous cell carcinoma," *International journal of radiation oncology, biology, physics*, vol. 95, pp. 368–376, 05 2016.
- [31] E. Thekkedath, S. Mikulic, F. Kandah, and S. Sheffield, "Treatment of sinonasal undifferentiated carcinoma with neoadjuvant chemotherapy and proton therapy," *Current Problems in Cancer: Case Reports*, vol. 2, p. 100032, 12 2020.
- [32] P. J. Doolan, M. Testa, G. Sharp, E. H. Bentfour, G. Royle, and H.-M. Lu, "Patient-specific stopping power calibration for proton therapy planning based on single-detector proton radiography," *Physics in Medicine and Biology*, vol. 60, no. 5, pp. 1901–1917, feb 2015. [Online]. Available: <https://doi.org/10.1088/0031-9155/60/5/1901>
- [33] C.-A. Collins-Fekete, S. Brousmiche, D. C. Hansen, L. Beaulieu, and J. Seco, "Pre-treatment patient-specific stopping power by combining list-mode proton radiography and x-ray CT," *Physics in Medicine & Biology*, vol. 62, no. 17, pp. 6836–6852, aug 2017. [Online]. Available: <https://doi.org/10.1088/1361-6560/aa7c42>
- [34] N. Krah, V. Patera, S. Rit, A. Schiavi, and I. Rinaldi, "Regularised patient-specific stopping power calibration for proton therapy planning based on proton radiographic images," *Physics in Medicine & Biology*, vol. 64, no. 6, p. 065008, mar 2019. [Online]. Available: <https://doi.org/10.1088/1361-6560/ab03db>
- [35] C. Gianoli, M. GÄppel, S. Meyer, P. Palaniappan, M. RÄrdler, F. Kamp, C. Belka, M. Riboldi, and K. Parodi, "Patient-specific ct calibration based on ion radiography for different detector configurations in 1h, 4h and 12c ion pencil beam scanning," *Physics in Medicine & Biology*, 2020. [Online]. Available: <http://iopscience.iop.org/article/10.1088/1361-6560/aba319>